RESEARCH ARTICLE

ADVANCED
MATERIALS
INTERFACES

Check for updates

www.advmatinterfaces.de

Surface Heterogeneity Affects Adsorption Selectivity for CO$_2$ Over CH$_4$ in Bare Mesostructured Silica with 2D Hexagonal Symmetry and Different Pore Size

Paola Carta* and Mariano Andrea Scorciapino*

Mesoporous silica-based materials are used as sorbents and supports in many fields. The ordered pore architecture of MCM-41, and the absence of interconnections, make it suitable as a model system. The surface is natively functionalized by many silanol groups, endowing the material with a polar surface to directly interact with the target species or to mount additional functional groups. Either bare or functionalized, surface silanol arrangement is crucial to material performance. In the case of CO$_2$ capture with amine-functionalized silica, silanol groups are responsible for fundamental H-bonds during chemisorption, but they also modulate the effect and weight of humidity on the material performance. In addition, the silanol groups can also tune the weight of physisorption over chemisorption. The relationship between these aspects and the textural features of mesostructured silica has not been addressed in detail. In this study, computer models are employed to investigate the adsorption capacity and selectivity of bare mesostructured silica with three different pore sizes. Results are rationalized in terms of silanol surface density and pore curvature. The importance of the energetic inequivalence between Q^3 and Q^2 sites on the silica surface is emphasized, as this causes adsorption behavior to deviate from ideality.

1. Introduction

Mesoporous silica-based materials are used as sorbents and supports in many fields, such as separation, capture, storage, and catalysis. The growing attention and interest for further development is due to the large surface area (up to 2000 m^2 g^{-1}) and the highly uniform pore size, beside the many approaches available to functionalize their surface for specific applications.[1–12]

P. Carta, M. A. Scorciapino
Department of Chemical and Geological Sciences
University of Cagliari
Cittadella Universitaria di Monserrato
SP 8 km 0.700, 09042 Monserrato, CA, Italy
E-mail: paola.carta94@unica.it; scorciapino@unica.it

The ORCID identification number(s) for the author(s) of this article can be found under https://doi.org/10.1002/admi.202300196

Among the mesostructured silica, MCM-41 and SBA-15 are the most widely investigated and employed ones, because of their regular 2D hexagonal array (P6mm space group symmetry) of highly uniform parallel mesopores, with a pore diameter of 2–10 and 5–30 nm, respectively.[1] SBA-15 also has a network of micropores (diameter <2 nm) interconnecting the mesopores. The ordered pore architecture of MCM-41, and the absence of interconnections, makes this material particularly suitable as a model system.

Mesostructured silica are not inert materials, as they natively present their surface functionalized by many silanol groups. These endow the material with a polar hydrophilic surface, with the silanol groups available to directly interact with the target species, or opening the possibility to mount an extreme variety of additional functional groups due to their reactivity.[3] Regardless co-condensation or a post-synthesis strategy is employed (e.g.: grafting and impregnation), the presence and arrangement of silanol groups is crucial, leading to different possible linkage of the functionalizing units, with possibly different reactivity. Rate and results of the functionalization process will depend on the surface silanol groups local concentration, steric factors and the diffusion limitation within the pores.[13,14]

Mesostructured silica is not often employed as bare materials, since the loading capacity and selectivity for a given species would rely only upon relatively weak interactions (van der Waals interactions and hydrogen-bonding), namely, upon physisorption. Functionalizing units are typically added on the surface to increase performance through more specific interactions and reactions, in terms of capacity and, especially, selectivity, depending on the goal. In general, outcomes of the functionalization process depend on the number of functional units, and one can expect that the larger the surface coverage, the higher the capacity and selectivity. However, other features of the material surface do play a role in different and sometimes subtle ways, such that golden rules for mesostructured silica functionalization still do not exist.

We focus here on the case of CO$_2$ separation as an example, due to the high attention of the scientific community and media to the technologies commonly referred to as Carbon Capture and

**ADVANCED
SCIENCE NEWS**

www.advancedsciencenews.com

**ADVANCED
MATERIALS
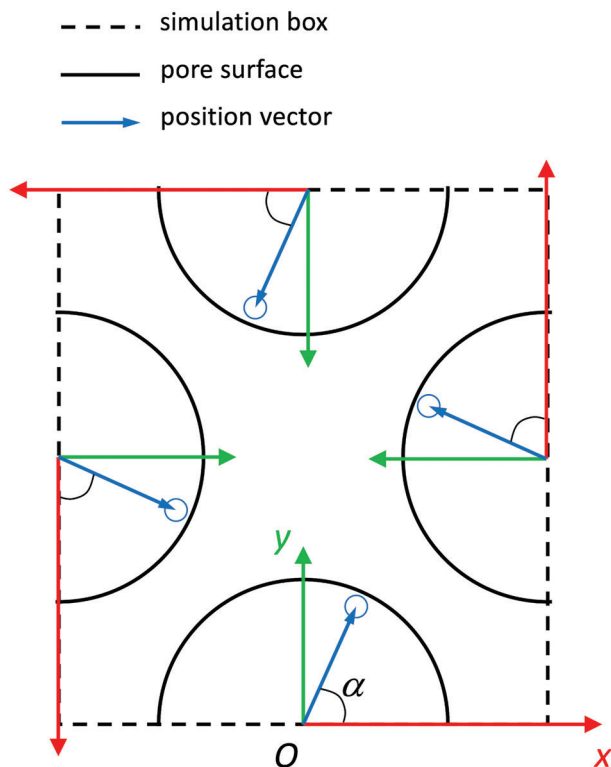INTERFACES**

www.advmatinterfaces.de

Figure 1. The xy-projection of the simulation box for a generic mesoporous material is schematically shown, together with the angle, α, used to describe gas molecule azimuthal position with respect to the pore surface for each of the four half-pores.

Utilization (CCU).[15] To enhance CO_2 adsorption performance of bare silica mesopores, amine functionalization, either by impregnation or grafting, has been widely employed.[16] In most of the investigations, primary and/or secondary amines reacted with CO_2 and formed carbamate species, which is a clear example of chemisorption. Not only the specific amine had large effect on the material performance, but also the amine loading and pore diameter did.[16,17] Even water vapor was found to affect CO_2 adsorption, sometimes with positive,[18,19] sometimes with negligible,[20] or with negative effects,[19] depending on the specific amine employed and related also to pore size and amine density. Extensive overview of mesostructured silica performance as CO_2 adsorbents is given by valuable recent reviews.[21–24]

Although the reaction mechanism was initially proposed to proceed as much as in liquid systems, such hypothesis has been challenged by both experimental and theoretical studies. Hydrogen bonds can be formed among nearest neighbors, both between grafted-amines pairs or between isolated amines and the flanking OH groups on the silica surface.[25,26] These interactions appear to be crucial to have chemisorption. When alkylamine groups are isolated and the alkyl chain is either too short or rigid to interact with the silanol groups on the silica surface, no chemisorption was observed.[27] In the recent literature, the complexity of the adsorbate-adsorbent system is becoming clear for CO_2 adsorption on amine-functionalized mesoporous silica. Several chemisorbed species are formed, even when just a single type of amine functionalizing unit is present. The different network-

ing of hydrogen bonds between the adduct being formed and either the surface silanol groups and/or the neighboring amines is extremely important.[28,29] For this reason, the impact of the overall amine loading, and, thus, of the number, density, and location of the remaining silanol groups, is great on the material performance.

The importance of the remaining surface silanol groups does not pertain only to their role during chemisorption, but they can also modulate the effect and weight of humidity on the material performance. On the basis of the proposed mechanisms, these hydrophilic surface groups would facilitate higher efficiencies of chemisorption by attracting water molecules. However, an excess of humidity could lead to water condensation inside the pores, preventing the access of CO_2 to the adsorption sites and worsening material performance.[19] In addition, the silanol groups can also tune the weight of physisorption over chemisorption. In fact, when the effect of temperature was investigated, the coexistence of both physical and chemical adsorption was emphasized.[30] By comparing CO_2 adsorption in bare and in amine-modified MCM-41, it has been shown that on the surface of the latter, the chemisorption of CO_2 occurs at low pressures (up to 0.1 bar), reaching a total amount of adsorbed gas significantly larger than that in the bare material at the same pressure. However, at larger pressures, the difference is not important, indicating that chemisorption is followed by physisorption after the saturation of the reactive amine groups, and that the amount of physisorbed CO_2 is not negligible.[31]

The relationship between these aspects and the textural features of the mesostructured silica has not been addressed in detail yet. In this work, computer models of MCM-41 have been generated, sharing the same P6mm mesostructure symmetry but with different pore diameters. By using a combination of Grand-Canonical Monte Carlo (GCMC) and Molecular Dynamics (MD) simulations, their adsorption capacity for either CO_2 and CH_4 have been investigated at 303 K and in the 1–10 atm pressure range, in order to observe the effect of changing the pore size. Both pure components and binary CO_2/CH_4 mixtures with different composition have been investigated, and the results from the atomistic computer simulations have been compared to the predictions provided by the application of the Ideal Adsorbed Solution Theory (IAST).[32] The adsorption capacity and the selectivity of the different models have been rationalized in terms of their microscopic details, unveiling interesting differences in the adsorption process that ultimately depend on silanol surface density and pore curvature. Deviations of the adsorption behavior from the ideality could be explained by focusing on the energetic inequivalence of the different adsorption sites, namely, Q^3 and Q^2 sites on the silica surface.[4,33–35] Such surface heterogeneity appears to promote selectivity for CO_2 over CH_4 at low CO_2 concentration, which is granted at low molar fraction and low (atmospheric) pressure.

2. Experimental Section

2.1. Simulation Box Preparation

The 3D structure of three different mesostructured silica was obtained as described in details elsewhere.[35] These three materials differed in the pore diameter, but shared the same 2D
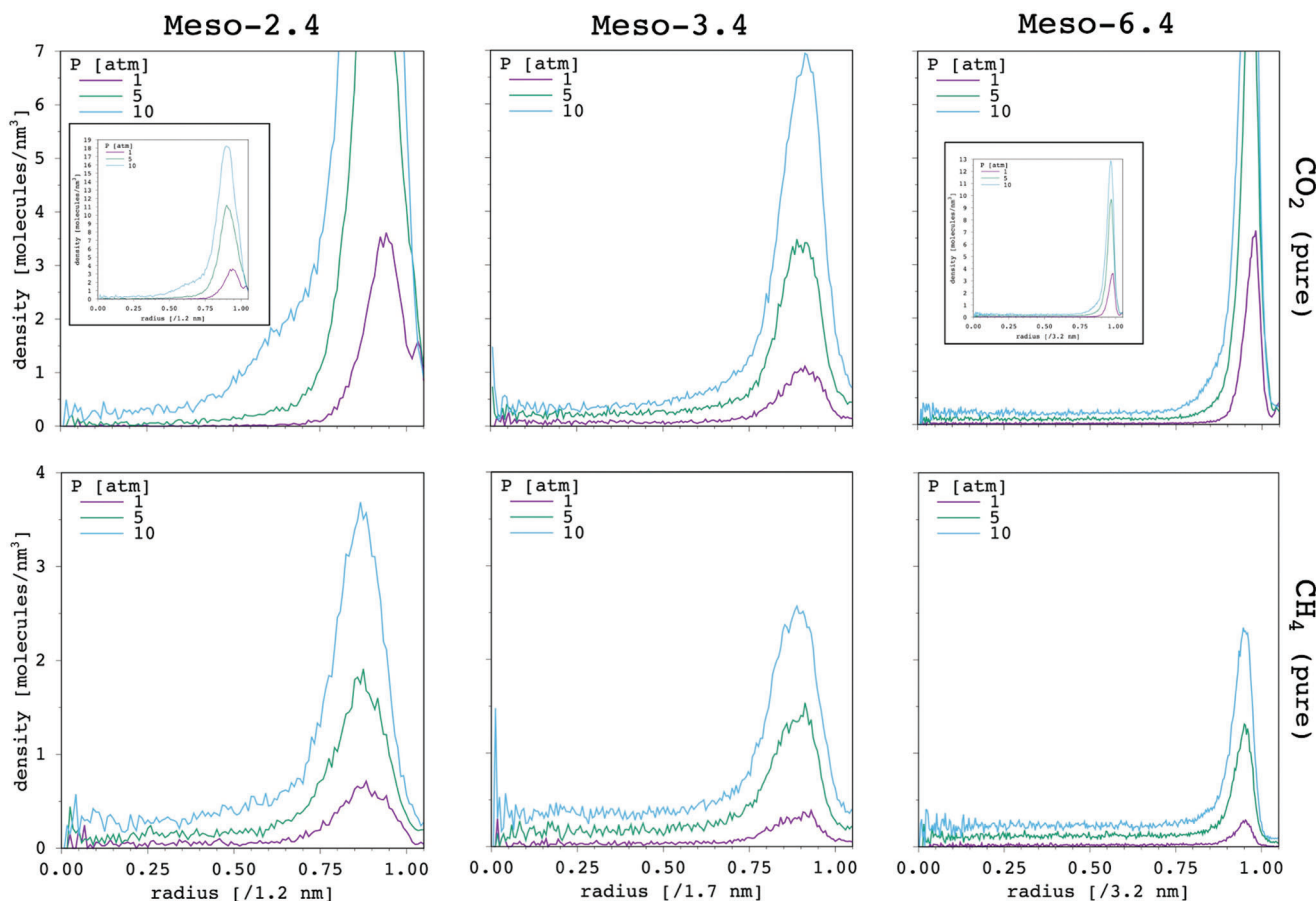
2300196 (2 of 12)

**ADVANCED
SCIENCE NEWS**

www.advancedsciencenews.com

**ADVANCED
MATERIALS
INTERFACES**
Open Access

www.advmatinterfaces.de

Figure 2. Density profile of pure CO_2 (top row) and CH_4 (bottom row) inside the pores of Meso-2.4 (left column), Meso-3.4 (middle column) and Meso-6.4 (right column) materials. Scaled pore radius is reported on x-axis (zero corresponds to the pore center), in order to compare materials with different pore size. For the sake of comparison, a few curves go beyond the selected upper limit of the y-axis. Full curves are shown in the corresponding inset.

hexagonal symmetry (P6mm space group) of identical parallel and non-interconnected cylindric mesopores. The small-angle XRD patterns for MCM-41[4,35] and for SBA-15 (unpublished data), provided the lattice spacing and space group symmetry of the mesophase. Correspondingly, the unit cell parameter (i.e., the interpore distance) for MCM-41 (4.4 nm) and SBA-15 (10.0 nm) was determined. Two models were built on the basis of MCM-41, with a pore-diameter of 2.4 and 3.4 nm on the basis of the reported BJH and DFT analysis of the same N_2-physisorption isotherm, respectively.[35] The third model was built on the basis of SBA-15, for which the mesopores diameter was as large as 6.4 nm. We decided to not include the micropores, to obtain an MCM-41 like material and to focus our attention on the weight of the mesopore size. **Table 1** summarizes the main geometrical and topological parameters of the three model materials investigated in this work. Periodic boundary conditions (PBC) were applied to all the three dimensions of the system.

Briefly, the unit cell of β-cristobalite[36] was replicated along the x, y, and z dimensions. Its density (2.3 g cm^{-3}) is close to the reported density of the amorphous silica (2.2 g cm^{-3}).[37] One half-pore was obtained in the middle of each of the four faces parallel to the z-axis, by eliminating the atoms within the proper cylindri-

cal volume (Table 1). The axis of the pores was perpendicular to the xy-plane.

The resulting unsaturated Si atoms were eliminated. The resulting isolated O atoms were eliminated too. The remaining surface O atoms were treated through an in-house computer code,[35] to possibly match the SS-NMR experimental $\frac{Q^2+Q^3}{Q^2+Q^3+Q^4}$

Table 1. Main parameters of the simulated mesostructured silica. Lengths are reported in nanometer units.

Model	Symmetry	a)d_{100}	b)a_0	c)d_p	d)w	Box edges [x,y,z]	e)Number of atoms
Meso-2.4f)	P6mm	3.8	4.4	2.4	2.0	$4.3 \times 7.9 \times 2.2$	3472
Meso-3.4g)	P6mm	3.8	4.4	3.4	1.0	$4.3 \times 7.9 \times 2.2$	2352
Meso-6.4	P6mm	8.7	10.0	6.4	3.6	$10.0 \times 17.2 \times 2.2$	15289

a) Lattice spacing; b) Interpore distance; c) Pore diameter; d) Wall thickness; e) Gas molecules are not included; f) This model was referred to as MCM-41/BJH in a previous publication;[35] g) This model was referred to as MCM-41/DFT in a previous publication.[35]
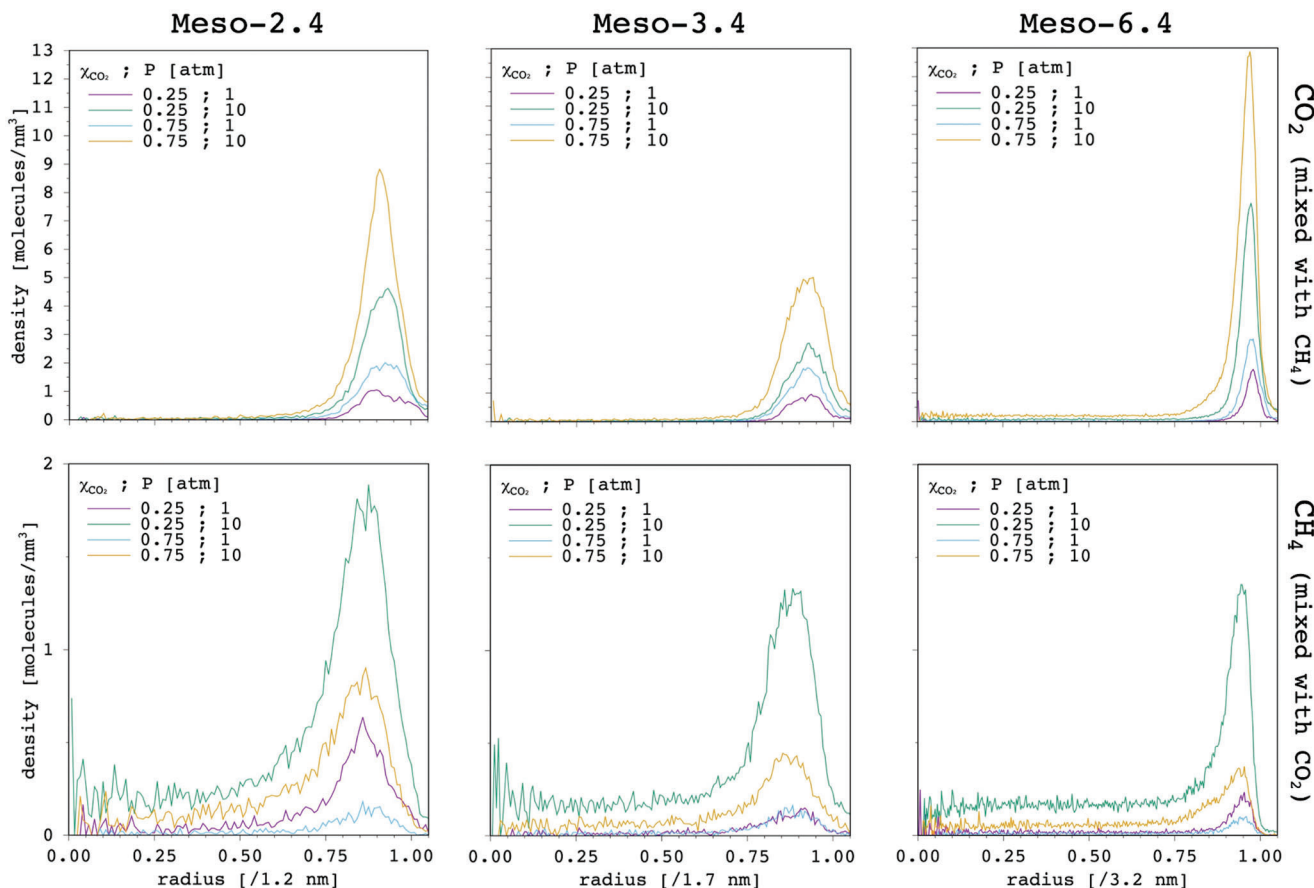
ADVANCED
SCIENCE NEWS

www.advancedsciencenews.com

ADVANCED
MATERIALS
INTERFACES
Open Access

www.advmatinterfaces.de

Figure 3. Density profile of CO_2 and CH_4 inside the pores of Meso-2.4 (left column), Meso-3.4 (middle column) and Meso-6.4 (right column) materials. Results of binary mixtures of the two gases are shown for selected compositions and pressure values. Scaled pore radius is reported on x-axis (zero corresponds to the pore center), in order to compare materials with different pore size.

ratio (the index refers to the number of —O—Si—O— linkages to the material bulk). In the case of Meso-2.4, all the surface O atoms were hydrogenated to obtain the surface —Si—OH groups. Although it does not strictly pertain to the present investigation, it is worth mentioning that such per-hydrogenation was not sufficient to reach the experimental $\frac{Q^2+Q^3}{Q^2+Q^3+Q^4}$ ratio.[35] In the case of Meso-6.3, per-hydrogenation was similarly applied, due to the lack of a real sample on which SS-NMR analysis could be performed (the model has is based on SBA-15 but has no micropores). In the case of Meso-3.4, a number of surface Si atoms were randomly selected to form new —Si—O—Si— bridges. The remaining surface O were hydrogenated, matching the SS-NMR experimental $\frac{Q^2+Q^3}{Q^2+Q^3+Q^4}$ ratio.[35]

Finally, the materials were subjected to the amorphization stage, i.e., a random maximum displacement of 0.5 Angstrom was applied to each atom. A thousand steps of energy minimization were performed with conjugate-gradients. The equilibration was performed in the NVT ensemble with classical Molecular Dynamics (MD) (2.0 fs time-step; temperature was gradually increased from 1 to 303 K along 20 ps, and then kept at 303 K for 100 ps). The Nose–Hoover thermostat was applied with a tdamp of 100. The velocity Verlet algorithm was used as reported by Tuckerman et al.[38] and by applying the equations of motion for-

mulated by Shinoda et al.[39] Positional restraints were applied to the O and Si atoms. The Shake algorithm[40] was applied to both O—H stretching and Si—O—H bending. No potential was applied to the torsion around Si—O bond. All the simulations were carried out with LAMMPS[41,42] (https://www.lammps.org).

2.2. Gas Adsorption Simulation

Gas molecules were inserted into the material's pores and the system was equilibrated at the given temperature (303 K) and pressure (1, 5 and 10 atm). Pure CO_2, pure CH_4, or a CO_2/CH_4 mixture with CO_2 molar fraction (χ_{CO_2}) of 0.25, 0.50 or 0.75, were considered. The MC simulation algorithm was applied for 2,500 steps in the Grand Canonical ensemble (GCMC), by attempting only gas molecules insertions and deletions inside the pores (1 of each kind on average at every step). MD followed in the NVT ensemble as described above for 75,000 steps (150 ps), by treating gas molecules as rigid bodies, while keeping the material still. This GCMC+MD scheme was iterated up to equilibrium, i.e., when the number of gas molecules fluctuated around a constant value for 100,000 GCMC consecutive steps, at least. New velocities were generated at each run (both GCMC and MD) by often changing the seed for the random number generator (both for

2300196 (4 of 12)

**ADVANCED
SCIENCE NEWS**

www.advancedsciencenews.com

**ADVANCED
MATERIALS
INTERFACES**
Open Access

www.advmatinterfaces.de

velocities and GCMC moves) to improve stochastic sampling of the phase space. Finally, the production MD run was carried out in the NVT ensemble for 1 ns.

2.3. Force-Field Potentials and Parameters

The $-Si-O-H$ surface groups were described with harmonic potential for bonds stretching and angle bending during the material preparation. The parameters reported by Bigot and Peuch[43] were used. Gas molecules were treated as rigid bodies. A sum of Lennard–Jones and Coulomb potentials were used to describe the non-bonded interactions, with the parameters by Furukawa et al.[44] A double cutoff was applied, with values of 12.0 and 14.0 Å. A long-range van der Waals tail correction was included.[45–47] The Particle-Particle Particle-Mesh method[48] was applied for long range electrostatics. A screening parameter of $\kappa = 3.2/\text{cutoff}$ and an upper bound of the reciprocal space summation at $K_{max} = \text{int}(\kappa L_{box}) + 1$ were used, as reported by Shah et al.[46,47] The TraPPE force-field[47] were applied to describe the gas molecules.

2.4. Trajectory Analysis

The density profile of gas molecules (each one localized at its center of mass) was reconstructed as a function of the pore radius with an in-house computer code.[35] The amount of adsorbed gas in $cm^3 g^{-1}$ was calculated as follows: the integral of the density profile was numerically calculated, the number of molecules was converted into moles, and the result was multiplied by the molar volume of the ideal gas at STP conditions and by the material's specific surface area (SSA). The latter was obtained as the solvent accessible area with PyMOL v2.5 (https://pymol.org/2/; "get area" tool; dot_density = 4; N_2 probe radius = 1.6 Å from Chemicalize https://chemicalize.com/ by ChemAxon http://www.chemaxon.com). When gas density at the pore center was not zero, density profiles were corrected to remove the bulk density contribution (ρ_b).[49–52] We used $\rho_b = \frac{m(r_p - 2p)^s}{(r_p - 2p)^s + p^s}$; $m \geq 0$; $p \geq 0$; $s = 2, 4, 6, \ldots$, where m is the maximum at $r_p \rightarrow 0$, p is the position of the falling point of inflection, and s modulates the slope at the inflection point. Adsorption selectivity of the species-i over the species-j is defined as $S_{i/j} = \frac{\chi_{a,i}/\chi_{g,i}}{\chi_{a,j}/\chi_{g,j}}$, where subscript a and g are used for the adsorbed and the gas phase, respectively. The Ideal Adsorbed Solution Theory (IAST)[32] has been employed by using the simulations of the pure components, to compare the results to those obtained through the simulations of the mixtures. The azimuthal position of gas molecules inside the pores was suitably defined by making use of the cylindrical coordinates in each of the four half-pores within the simulation box. Molecular center of gravity corresponds to the position of the C atom for both CO_2 and CH_4, and the azimuthal angle, α, is shown in **Figure 1** in each of the half-pores, as it was determined through an in-house computer code.

Radial distribution functions were obtained with LAMMPS, as well as the gas molecules energy. The diffusion coefficients of gas molecules along the pores were calculated as $D = \frac{\left\langle \left(r_i(t) - r_i(t_0)\right)^2 \right\rangle}{2d(t - t_0)}$,

where r are the coordinates of the center of mass of the gas molecules of the given type, t_0 is the starting time, and d is the number of dimensions over which the analysis is performed. For this analysis, the MD trajectory has to be unwrapped, i.e.: coordinate reflections due to the PBC have to be removed and the real displacement needs to be recovered.

3. Results and Discussion

Progressive CO_2 and CH_4 adsorption are observed with increasing pressure, regardless pure gasses or binary mixtures are simulated. In the present context, silica-based materials are studied in the absence of any additional functional unit on their surface, beside the native silanol groups. Thus, the adsorption is based on relatively weak non-bonded interactions, i.e.: physisorption. **Figure 2** shows the gas density profiles inside the pores of the three materials for the two pure gases at different pressure.

The larger affinity of CO_2 over CH_4 is evident, regardless of the pore size and the pressure. For different molecules, it is well recognized that the smaller the pore radius, the lower the pressure needed to have condensation inside the pores.[53–55] In fact, maximum density was observed for pure CO_2 in Meso-2.4 at 10 bar (Figure 2, top left panel), where, beside the main adsorption peak attributable to the monolayer formed on the pore surface, a shoulder is clearly present at shorter values of the radius. This is indicative of an almost saturated CO_2 adsorbed monolayer, and the consequent initial formation of a second layer of gas molecules on top of it, similarly to what was observed in the case of N_2.[35] Inspection of the simulation trajectory confirmed this observation. In all the other investigated cases and conditions, density profiles are remarkably lower and only the main adsorption peak is observed. This indicates that the adsorbed monolayer is far from saturation, that the spreading pressure of gas molecules in the monolayer is rather low, as well as the intermolecular interactions, and the Ideal Adsorbed Solution Theory (IAST) should be applicable.[32]

The same observations and comparisons do apply to the CO_2/CH_4 binary mixture simulations. The corresponding gas density profiles for selected pressures and compositions are shown in **Figure 3**.

The density of each component in the adsorbed phase increases with the total pressure and with the corresponding molar fraction. The density of each component is always lower than observed in the simulations of the corresponding pure gas at the same pressure.

Adsorption capacity of the three materials for pure CO_2 and CH_4 is shown in **Figure 4**, together with the selectivity resulting from the simulations of their mixture with different composition.

All the three materials share a clear selectivity for CO_2 over CH_4, as shown by the larger adsorbed amount of the former at all pressures (Figure 4a). By virtue of the different pore radius and wall thickness, the three materials have a remarkably different SSA, which is 345, 689, and 192 $m^2 g^{-1}$ for Meso-2.4, Meso-3.4, and Meso-6.4, respectively. As it was already observed in the case of N_2 adsorption,[35] this difference is expected to provide a rather different adsorption capacity, since the lower the SSA, the lower the number of surface silanol groups. In fact, the expected trend is followed by CH_4 (Figure 4a) at all pressures, while the similar
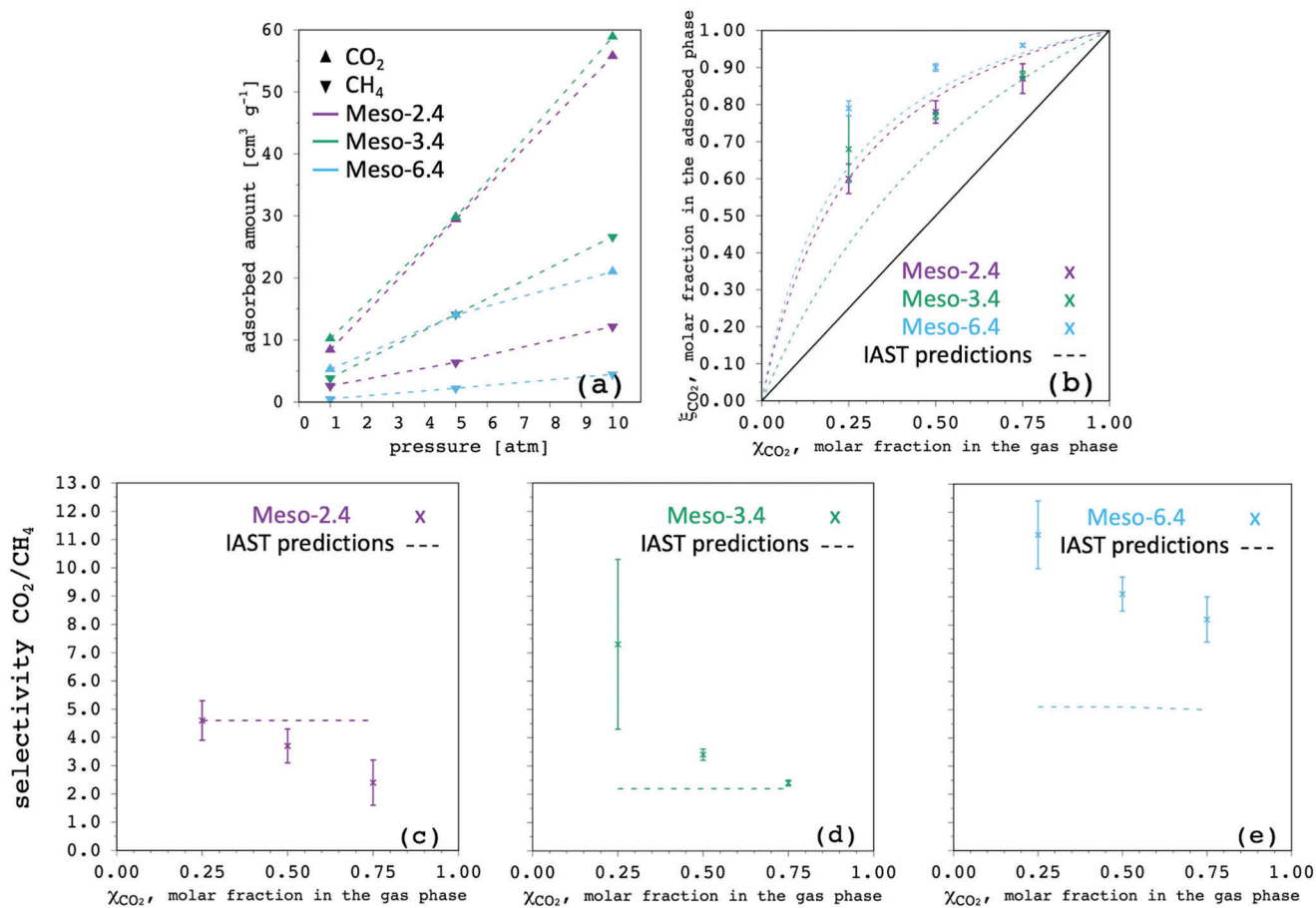
**ADVANCED
SCIENCE NEWS**

www.advancedsciencenews.com

**ADVANCED
MATERIALS
INTERFACES**
Open Access

www.advmatinterfaces.de

Figure 4. a) CO_2 and CH_4 adsorption capacity from simulations of the pure gases in the Meso-2.4, Meso-3.4 and Meso-6.4 models. b) Molar fraction of CO_2 in the adsorbed layer, ξ_{CO_2}, is compared to its molar fraction in the gas phase, χ_{CO_2}, from the simulations of CO_2/CH_4 binary mixtures in the three model materials. c–e) Selectivity of the three model materials for CO_2 over CH_4. Error bars (b–e) represent the standard deviation of the results obtained at 1, 5, and 10 atm. a) Dashed lines (b–e) show the results from the application of the IAST model[32] to the data of the pure gases.

capacity of the Meso-2.4 and Meso-3.4 materials for CO_2 is quite surprising, at a first glance. However, as shown above (Figure 2), it has to be stressed that the Meso-2.4 model is found in a different adsorption regime in the simulated pressure range, with CO_2 approaching and surpassing the first-monolayer saturation point.

A linear trend was observed for the adsorbed amount vs. pressure (Figure 4a), which is in agreement with the literature at pressure larger or equal than 1 atm,[56–58] while marked curvature is observed at lower pressure, but especially at a lower temperature.[58,59] The obtained absorbed amounts are in good agreement with other reports, as summarized in **Table 2**.

The observed linearity of the adsorbed amount vs. pressure (Figure 4a), tempted us to apply the IAST model[32] to estimate the molar fractions in the adsorbed phase (Figure 4b) and selectivity for CO_2 over CH_4 (Figure 4c–e), on the basis of the simulations of the two pure gases, similarly to what would be performed on the experimental adsorption isotherm of the two pure components. However, the results obtained from the simulations of the CO_2/CH_4 mixtures show significant deviations from the ideal IAST predictions (Figure 4b–e).

The latter assesses that selectivity is larger for Meso-2.4 (4.6) than Meso-3.4 (2.2). However, we are convinced that this result for Meso-2.4 is largely biased by the fact that the corresponding data for pure CO_2 were obtained in proximity of the first-monolayer saturation, as mentioned, resulting in selectivity overestimation. In fact, for a reliable IAST analysis, the pure component isotherms should be measured accurately at low surface coverage, because the integration needed to determine the spreading pressure is very sensitive to the very initial portion of the adsorption isotherm.[32] Thus, without emphasizing the values obtained from IAST, the important point is that the latter inherently predicts a constant selectivity as a function of mixture composition (Figure 4), while all the investigated materials exhibit a significant variation as a function of CO_2 molar fraction in the gas phase, χ_{CO_2}. More specifically, selectivity increases with decreasing χ_{CO_2} in all the investigated materials.

It is worth noting that selectivity of the two materials with a similarly narrow pore size becomes comparable with increasing χ_{CO_2}, both approaching the IAST value obtained for Meso-3.4, which is in agreement with experimental data.[61,62] Conversely, at the lowest χ_{CO_2}, Meso-3.4 becomes more selective and, in addition, while Meso-2.4 selectivity does not result to be

**ADVANCED
SCIENCE NEWS**

www.advancedsciencenews.com

**ADVANCED
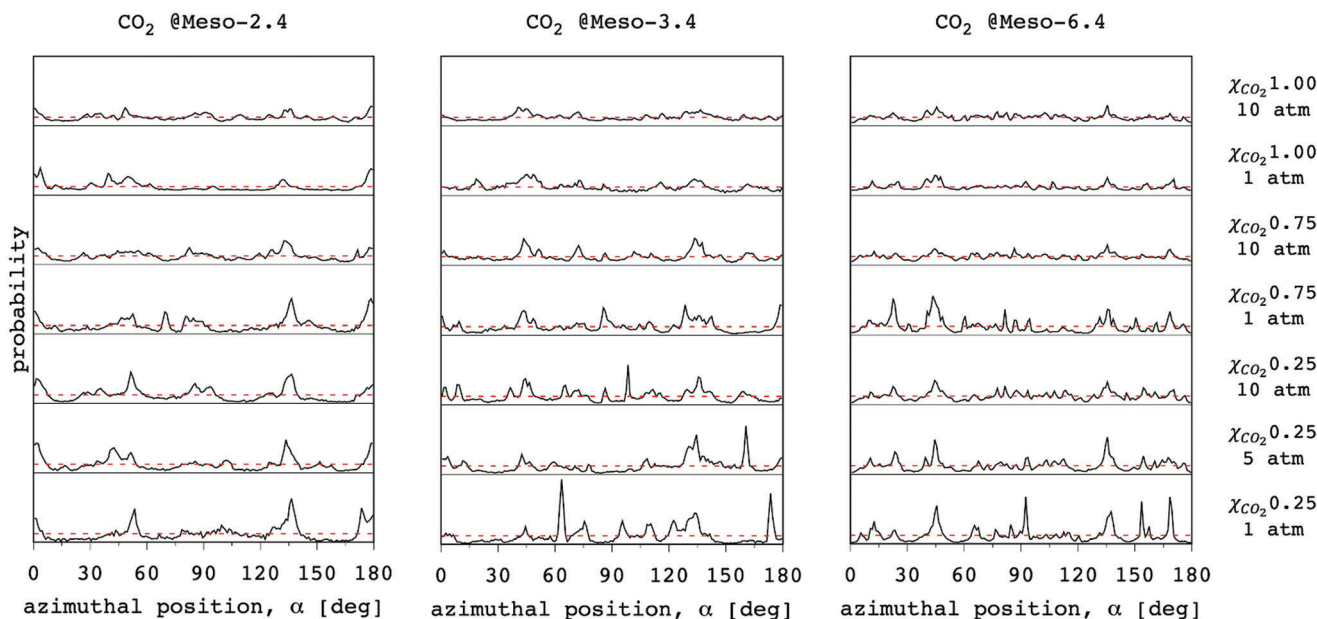MATERIALS
INTERFACES**

www.advmatinterfaces.de

Figure 5. Probability distribution of the azimuthal position (Figure 1) of CO_2 molecules inside the pores of Meso-2.4, Meso-3.4, and Meso-6.4 material models for selected compositions of the binary CO_2/CH_4 mixtures and for selected pressure values. A black solid horizontal line is used as the baseline of each distribution. Red dashed lines represent a perfectly homogenous surface coverage.

Table 2. The adsorbed amounts of pure CO_2 obtained for the three mesostructured material models investigated in this work are compared with data from the literature.

Pressure [atm]	Temperature [K]	Amount [cm³ g⁻¹]	Pore size [nm]	Reference
1	298	~ 18	1.1	[60]
1	298	~ 13	3.1	[30]
1	298	~ 15	3.4	[56]
1	298	~ 15	3.6	[56]
1	303	8	2.4	This work
1	303	10	3.4	This work
1	303	5	6.4	This work
1	318	≈8	5.1	[57]
5	298	≈56	3.4	[56]
5	298	≈56	3.6	[56]
5	303	29	2.4	This work
5	303	30	3.4	This work
5	303	14	6.4	This work
5	318	≈30	5.1	[57]
10	298	≈88	3.4	[56]
10	298	≈88	3.6	[56]
10	303	56	2.4	This work
10	303	59	3.4	This work
10	303	21	6.4	This work

particularly sensitive to the applied pressure within the 1–10 atm range, Meso-3.4 shows large selectivity increase with decreasing the pressure. On the other hand, Meso-6.4, with the largest pore size, results in a larger selectivity at all gas mixture compositions but, similarly to Meso-2.4, it is virtually insensitive to the applied pressure within the 1–10 atm range.

Briefly, IAST is based on the assumption of an ideal adsorption of the gas mixture: i) The adsorbent is thermodynamically inert; ii) The adsorbent has a temperature-invariant area and such area is the same for all the adsorbates; iii) Gibbs definition of adsorption applies; iv) Low surface coverage, i.e., low gas spreading pressure.[32] In these conditions, the Langmuir model is typically applicable, which implies that adsorption takes place at well-defined sites on the adsorbent surface, that adsorption sites are energetically equal (and each site accommodates only one adsorbate molecule), and that there is no lateral interaction between adsorbed molecules.[63] Molecule density in our simulations of the mixtures is rather low (Figure 3), especially at the lowest pressure and the lowest χ_{CO_2}, so one can expect an ideal adsorption. Conversely, at the lowest CO_2 coverage, the largest selectivity and the largest deviation from ideality is found. Among all the above-mentioned assumptions, the energetic equivalence of the adsorption sites, and the absence of lateral interactions in the adsorbed layer attracted our attention.

Figure 5 shows the probability distribution of the azimuthal position of CO_2 molecules inside the pores, as defined in Figure 1. Overall, the presence of some preferential adsorption sites emerges, as coverage probability is not homogenous over the pore surface. This is particularly evident the less CO_2 amount is adsorbed on the pore surface, i.e., with decreasing χ_{CO_2} and pressure for all the materials. Coverage probability becomes more and more homogeneous with increasing the amount of CO_2, up to the results obtained for the pure gas. The adsorbate molecules are physiosorbed on the silica surface and, in contrast to the Langmuir model, they are not firmly bound to a given hydroxyl group. Beside the equilibrium between the bound
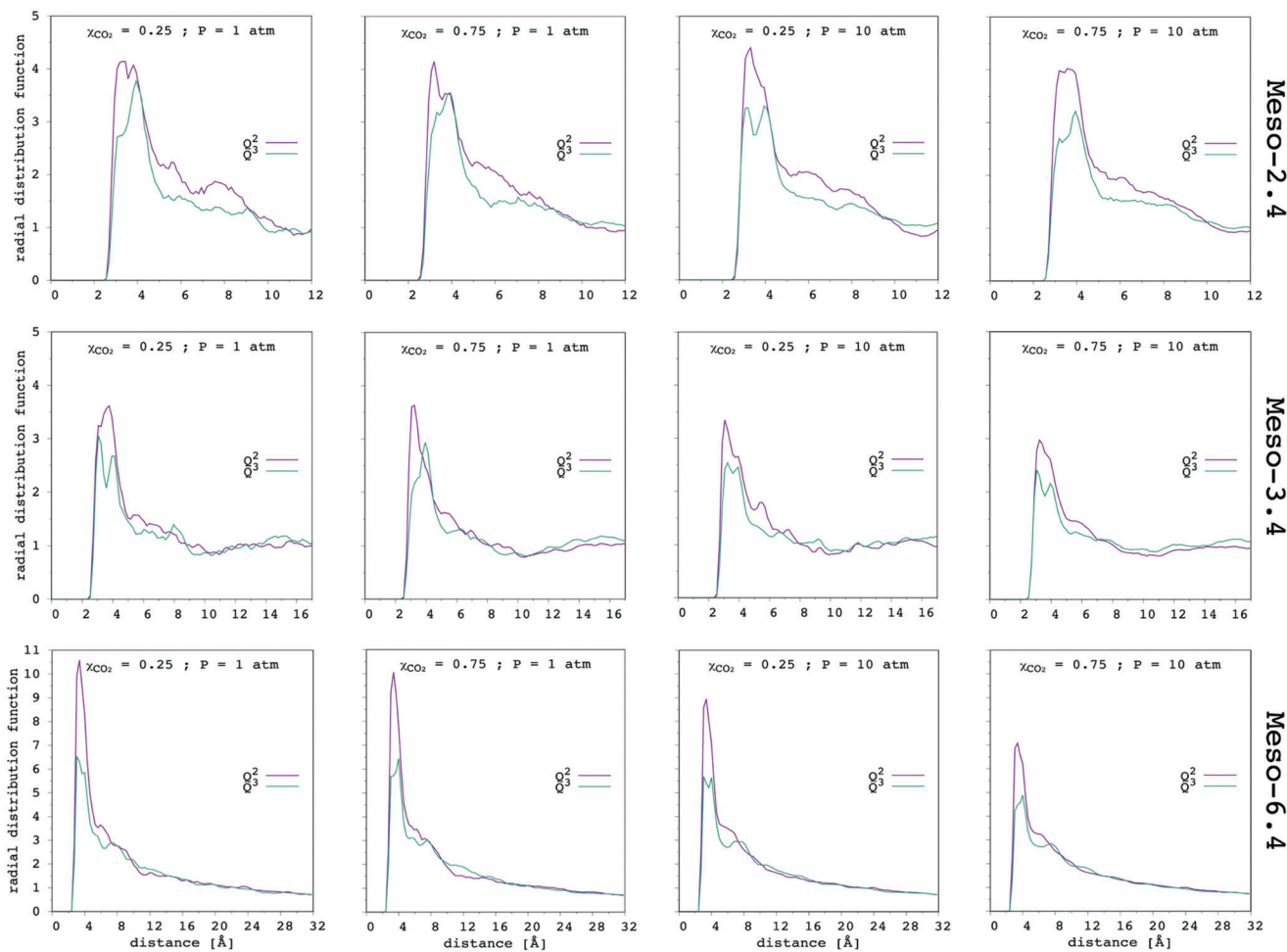
Figure 6. The radial distribution function (selected cases) computed for the distance between the hydroxyl O and the carbon dioxide C atom. The Q^3 and Q^2 sites are separately considered.

(adsorbed phase) and unbound (gas phase) state, molecules can sometimes slide on the surface, hopping from one site to the next, along the simulation. Overall, preferred sites are populated by the adsorbate with significantly larger frequency than other lower probability locations, when CO_2 amount is low. By increasing the latter, chances of finding unoccupied preferential sites along the dynamic trajectory inherently decreases for each CO_2 molecule and, therefore, occupancy of the lower affinity locations increases, which is reflected by a more and more homogenous coverage probability distribution (Figure 5). Although this general picture emerges for all the materials, Figure 5 shows how coverage probability in Meso-2.4 is hardly affected, being comparable at all pressures with 0.25 CO_2 molar fraction (even at 0.75 molar fraction and 1 atm). Similarly, also Meso-6.4 coverage is hardly affected by pressure, but surface coverage appears to be much more inhomogeneous. Differently, Meso-3.4 is much more sensitive to the CO_2 loading, with homogeneity of coverage probability in between Meso-2.4 and Meso-6.4.

Surface of mesostructured silica materials are not necessarily uniform, indeed, as different types of chemically inequivalent Si atoms are present. These are usually referred to as Q^3 and Q^2 on the basis of the number of —Si—O—Si— bridges with the bulk ma-

terial and, as a consequence, they are characterized by a single or two hydroxyl groups, respectively.[4,33–35] The radial distribution function (RDF) of CO_2 (position of the C atom) around either Q^3 or Q^2 hydroxyl groups (position of the O atom) are shown in **Figure 6** for the cases with the largest and the smallest χ_{CO_2} and pressure.

The probability of CO_2 interaction with Q^2 sites is larger than with Q^3 sites, at all molar fractions and pressures. The distance of the tallest peaks is compatible with H-bonding interactions for both sites, with Q^2 always showing larger probability at the shortest distance. The larger affinity of CO_2 for Q^2 sites is probably due to the presence of two geminal hydroxyl groups instead of the single one at Q^3 sites. The RDFs show that the surface of mesostructured silica can be thermodynamically heterogenous, causing the behavior of sorbates to deviate from ideality. **Figure 7** shows the distribution of the non-bonded energy ($U_{VdW} + U_{electrostatics}$) of the CO_2 molecules for the same selected cases reported in Figure 6.

Energy distributions were calculated for all CO_2 (or CH_4) molecules together, either those interacting with Q^2 and Q^3 sites. On average, the larger the fraction of molecules interacting with the most favorable Q^2, the lower the molecular energy.
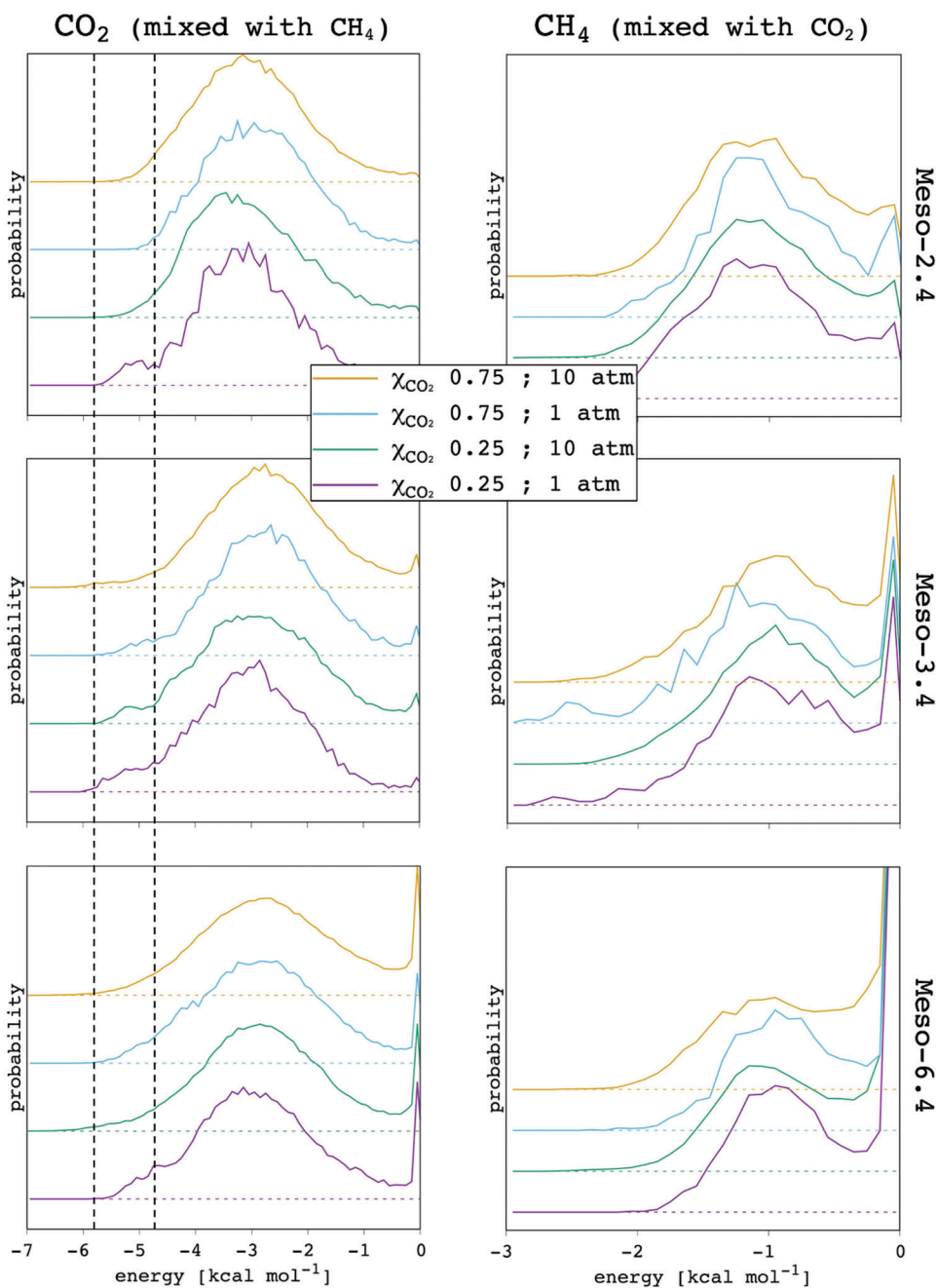
**ADVANCED
SCIENCE NEWS**

www.advancedsciencenews.com

**ADVANCED
MATERIALS
INTERFACES**
Open Access

www.advmatinterfaces.de

Figure 7. Distribution of the non-bonded molecular energy ($U_{VdW} + U_{electrostatics}$) of CO_2 and CH_4 as binary mixture (selected cases) inside the pores of Meso-2.4, Meso 3.4, and Meso-6.4 model materials. The two dashed lines in the panels on the left-hand side are intended just as reference to focus the lowest energy shoulder.

In agreement with the distribution of the azimuthal angle inside the pores (Figure 5), a progressive reduction of the low energy tail and concomitant increase of the high energy tail is observed for CO_2 energy distribution with increasing either χ_{CO_2} and/or pressure. This is especially marked in the case of Meso-2.4, which shows a clear lowest energy shoulder only at the lowest χ_{CO_2} and pressure. The evolution of the energy distribution is more gradual in Meso-3.4. The energy profile barely changes in Meso-6.4. This, together with RDFs (Figure 6), bolsters

the conclusion that CO_2 molecules preferentially adsorb at Q^2 sites.

All the observed differences between the three model materials correlates with the different S_{CO_2/CH_4} (Figure 4) and suggest that selectivity depends on the fraction of CO_2 molecules exploiting the most favorable adsorption sites available. It appears that this condition is easier or more pronounced in Meso-6.4 > Meso-3.4 > Meso-2.4, as reflected by the largest selectivity at low CO_2 loadings. Conversely, when CO_2 amount is

2300196 (9 of 12)

**ADVANCED
SCIENCE NEWS**

www.advancedsciencenews.com

**ADVANCED
MATERIALS
INTERFACES**
Open Access

www.advmatinterfaces.de

increased by molar fraction and/or pressure, the increasing density in the adsorbed layer forces gas molecules to spread over the surface, making progressively more difficult to optimally exploit all the most favorable sites. It is interesting to note how Meso-3.4 and Meso-2.4, with comparable pore size, in fact, becomes comparable in terms of selectivity. For the sake of completeness, also CH_4 shows preferential interaction with the Q^2 sites (RDFs not shown), but the non-bonding energy is very small, when compared to CO_2 (Figure 7) and does not change significantly as a function of molar fraction and pressure, indicating that CH_4 competition for adsorption with respect to CO_2 is negligible.

Summarizing all the results presented so far, the presence of two types of adsorption sites with different affinity for the species of interest, CO_2 in this case, determines a deviation from ideality. Selectivity is enhanced with decreasing the molar fraction of that species and the total pressure. The Q^2:Q^3 ratio is 0.45, 0.55, and 0.40, in Meso-2.4, Meso-3.4, and Meso-6.4, respectively. In addition, the different pore curvature affects the surface density of the Q^2. By virtue of its smallest pores, Meso-2.4 surface is characterized by the highest curvature, which is reflected by the largest density of Q^2 sites, which is 5.2 μmol m^{-2}. The value is comparable in Meso-3.4, i.e., 4.9 μmol m^{-2}, despite its surface area is larger than in Meso-2.4. This is due to the significantly larger number of Q^2 sites in Meso-3.4, which explains the higher S_{CO_2/CH_4} at low χ_{CO_2} and pressure. On the other hand, Q^2 sites are more separated on the pore surface of Meso-6.4. The smallest curvature contributes to the Q^2 density of 4.2 μmol m^{-2}. Occupancy of the less dense Q^2 sites by CO_2 is higher and this is reflected by the largest selectivity of Meso-6.4 at all molar fractions and pressures, although the relative number of Q^2 sites is the lowest.

For the sake of completeness, **Figure 8** shows the adsorption capacity of the three materials at $\chi_{CO_2} = 0.25$, where the correlation with the SSA is evident for both the gases.

The overall performance of the material is clearly dependent on different factors. While selectivity is the largest in Meso-6.4, its smallest SSA provides a lower CO_2 adsorption capacity than Meso-3.4. Definitely, the intermediate pore size of the latter makes the material sufficiently selective, while granting a large SSA. It is worth mentioning that such a nonmonotonic trend of the adsorption capacity as a function of the pore size was also reported for a series of SBA-15 samples.[16] However, when this type of materials are intended as gas filters, molecule dynamics inside the pores and flux density are very important. Permeability is directly proportional to both sorbent-sorbate affinity and sorbate diffusion coefficient. We focused our analysis on the cases of high selectivity (and comparable molecule density, by which molecule dynamics is greatly affected), which is $\chi_{CO_2} = 0.25$ at 1 atm. Results of the diffusion coefficient of both CO_2 and CH_4 are shown in **Figure 9**.

Regardless of the pore size, CO_2 has a lower diffusion coefficient than CH_4 in all the investigated cases, by virtue of its stronger interactions with the material surface. The diffusion of both gases increases with increasing the pore size but, whereas CH_4 shows an almost linear increase, CO_2 clearly does not. The lower the ratio between the diffusion coefficient of CO_2 and CH_4, the better the separation performance of the material. Thus, also from this point of view, the intermediate pore size mate-
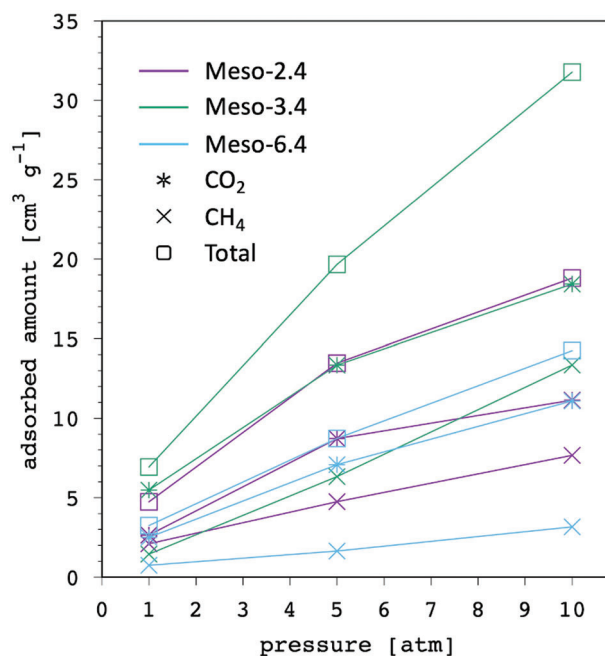

Figure 8. Adsorption capacity of CO_2, CH_4, and the total gas as a function of pressure for Meso-2.4 and Meso-3.4 model materials with $\chi_{CO_2} = 0.25$.

rial, Meso-3.4, appears to be the best one from this comparative study.

4. Conclusion

Three bare mesostructured silica-based materials with different mesopore size and no microporosity and have been compared through computer simulations. The adsorption capacity and selectivity for CO_2/CH_4 binary mixtures have been investigated with focus on atmospheric pressure. The results show that, while overall capacity is proportional to the specific surface area, deviation from adsorption ideality can lead to important differences in terms of selectivity. This is strictly related to the microscopic details of the pore surface, including pore curvature and the surface density of the adsorption sites. In particular, thermodynamic heterogeneity of the surface causes adsorption behavior to deviate from ideality. Heterogeneity is provided, in the present case, by the presence of chemically inequivalent surface silicon atoms, namely, Q^2 and Q^3. Selectivity increases when conditions allow the gas to spread on the surface and to occupy the majority of the most favorable sites. For the sake of completeness, it has to be noted that the number of Q^2 sites is typically lower in real samples[4,35] than it was in the presented computer models. This choice was made to emphasize surface heterogeneity and investigate its role, on the one hand, but it also showed how it is important to include all the experimental available information in the computer models, on the other. As far as we are aware, the ratio between $(Q^2+Q^3)/Q^4$, and the ratio between Q^2 and Q^3 are virtually never taken into account in the construction of computer models of silica-based materials.
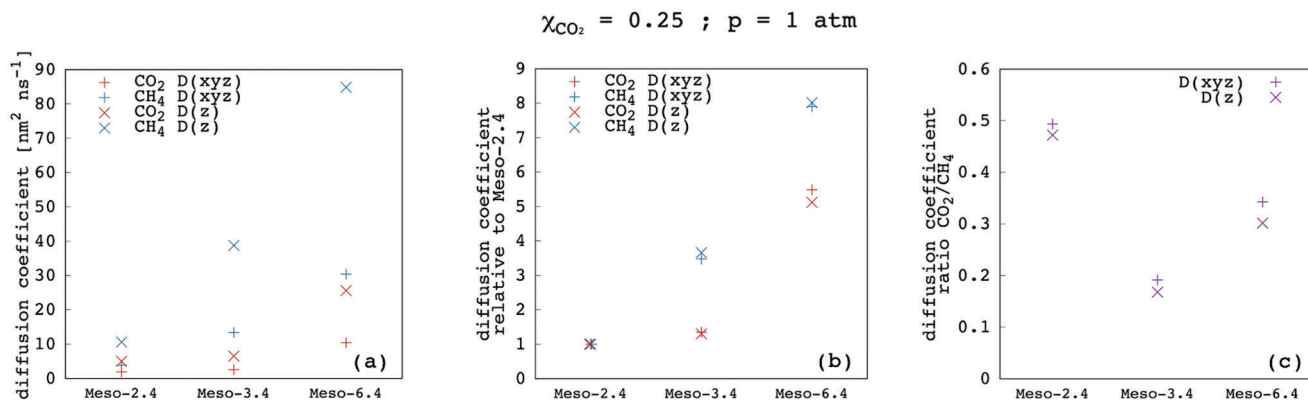
$$\chi_{CO_2} = 0.25 \; ; \; p = 1 \; atm$$

Figure 9. a) Diffusion coefficient of CO_2 and CH_4 inside Meso-2.4, Meso-3.4, and Meso-6.4 model materials at $\chi_{CO_2} = 0.25$ and 1 atm are shown. Either all the three Cartesian coordinates or only the z-coordinate (pore axis) were considered in the calculations. In b), each diffusion coefficient is divided by the corresponding value in the Meso-2.4 material. In c), the ratio between CO_2 and CH_4 diffusion coefficient is reported.

Conflict of Interest

The authors declare no conflict of interest.

Data Availability Statement

The data that support the findings of this study are available from the corresponding author upon reasonable request.

[1] Z. A. ALOthman, *Materials* **2012**, *5*, 2874.
[2] C. T. Kresge, M. E. Leonowicz, W. J. Roth, J. C. Vartuli, J. S. Beck, *Nature* **1992**, *359*, 710.
[3] J. A. S. Costa, R. A. de Jesus, D. O. Santos, J. B. Neris, R. T. Figueiredo, C. M. Paranhos, *J. Environ. Chem. Eng.* **2021**, *9*, 105259.
[4] M. A. Vacca, C. Cara, V. Mameli, M. Sanna Angotzi, M. A. Scorciapino, M. G. Cutrufello, A. Musinu, V. Tyrpekl, L. Pala, C. Cannas, *ACS Sustainable Chem. Eng.* **2020**, *8*, 14286.
[5] B. G. Trewyn, I. I. Slowing, S. Giri, H.-T. Chen, V. S.-Y. Lin, *Acc. Chem. Res.* **2007**, *40*, 846.
[6] C. Cara, V. Mameli, E. Rombi, N. Pinna, M. Sanna Angotzi, D. Nižňanský, A. Musinu, C. Cannas, *Microporous Mesoporous Mater.* **2020**, *298*, 110062.
[7] M. S. Angotzi, V. Mameli, C. Cara, K. B. L. Borchert, C. Steinbach, R. Boldt, D. Schwarz, C. Cannas, *Nanoscale Adv.* **2021**, *3*, 6100.
[8] E. Rombi, M. G. Cutrufello, C. Cannas, M. Casu, D. Gazzoli, M. Occhiuzzi, R. Monaci, I. Ferino, *Phys. Chem. Chem. Phys.* **2009**, *11*, 593.
[9] S. Varghese, M. G. Cutrufello, E. Rombi, C. Cannas, R. Monaci, I. Ferino, *Appl. Catal., A* **2012**, *443*, 161.
[10] C. Cara, F. Secci, S. Lai, V. Mameli, K. Skrodczky, P. A. Russo, F. Ferrara, E. Rombi, N. Pinna, M. Mureddu, C. Cannas, *J. CO2 Util.* **2022**, *62*, 102066.
[11] P. Bhanja, M. Sasidharan, A. Bhaumik, *J. Nanosci. Nanotechnol.* **2016**, *16*, 9223.
[12] A. Dutta, M. Nandi, M. Sasidharan, A. Bhaumik, *ChemPhysChem* **2012**, *13*, 3218.
[13] M. H. Lim, A. Stein, *Chem. Mater.* **1999**, *11*, 3285.
[14] X. S. Zhao, G. Q. Lu, A. K. Whittaker, G. J. Millar, H. Y. Zhu, *J. Phys. Chem. B* **1997**, *101*, 6525.
[15] I. Ghiat, T. Al-Ansari, *J. CO2 Util.* **2021**, *45*, 101432.
[16] J. A. Cecilia, E. Vilarrasa-García, R. Morales-Ospino, M. Bastos-Neto, D. C. S. Azevedo, E. Rodríguez-Castellón, *Adsorption* **2020**, *26*, 225.
[17] S. Choi, J. H. Drese, C. W. Jones, *ChemSusChem* **2009**, *2*, 796.
[18] Y. Belmabkhout, R. Serna-Guerrero, A. Sayari, *Ind. Eng. Chem. Res.* **2010**, *49*, 359.
[19] S. A. Didas, A. R. Kulkarni, D. S. Sholl, C. W. Jones, *ChemSusChem* **2012**, *5*, 2058.
[20] X. Wang, V. Schwartz, J. C. Clark, X. Ma, S. H. Overbury, X. Xu, C. Song, *J. Phys. Chem. C* **2009**, *113*, 7260.
[21] J. A. S. Costa, R. A. de Jesus, D. O. Santos, J. F. Mano, L. P. C. Romão, C. M. Paranhos, *Microporous Mesoporous Mater.* **2020**, *291*, 109698.
[22] A. A. Azmi, M. A. A. Aziz, *J. Environ. Chem. Eng.* **2019**, *7*, 103022.
[23] S. S. Fatima, A. Borhan, M. Ayoub, N. Abd Ghani, *J. Mol. Liq.* **2021**, *338*, 116913.
[24] E. E. Ünveren, B. Ö. Monkul, Ş. Sarıoğlan, N. Karademir, E. Alper, *Petroleum* **2017**, *3*, 37.
[25] J. C. Hicks, R. Dabestani, A. C. Buchanan, C. W. Jones, *Chem. Mater.* **2006**, *18*, 5022.
[26] J. C. Hicks, C. W. Jones, *Langmuir* **2006**, *22*, 2676.

[27] N. A. Brunelli, S. A. Didas, K. Venkatasubbaiah, C. W. Jones, *J. Am. Chem. Soc.* **2012**, *134*, 13950.

[28] L. Mafra, T. Čendak, S. Schneider, P. V. Wiper, J. Pires, J. R. B. Gomes, M. L. Pinto, *J. Am. Chem. Soc.* **2017**, *139*, 389.

[29] M. W. Hahn, J. Jelic, E. Berger, K. Reuter, A. Jentys, J. A. Lercher, *J. Phys. Chem. B* **2016**, *120*, 1988.

[30] S. Ahmed, A. Ramli, S. Yusup, M. Farooq, *Chem. Eng. Res. Des.* **2017**, *122*, 33.

[31] M. R. Mello, D. Phanon, G. Q. Silveira, P. L. Llewellyn, C. M. Ronconi, *Microporous Mesoporous Mater.* **2011**, *143*, 174.

[32] A. L. Myers, J. M. Prausnitz, *AIChE J.* **1965**, *11*, 121.

[33] E. Lippmaa, M. Maegi, A. Samoson, G. Engelhardt, A. R. Grimmer, *J. Am. Chem. Soc.* **1980**, *102*, 4889.

[34] M. Luhmer, J. B. d'Espinose, H. Hommel, A. P. Legrand, *Magn. Reson. Imaging* **1996**, *14*, 911.

[35] P. Carta, C. Cara, C. Cannas, M. A. Scorciapino, *Adv. Mater. Interfaces* **2022**, *9*, 2201591.

[36] *Zeitschrift für Kristallographie – Crystalline Materials* **1973**, *138*, 274.

[37] D. R. Lide, *CRC Handbook of Chemistry and Physics*, Taylor And Francis, Boca Raton (FL) – USA **2007**.

[38] M. E. Tuckerman, J. Alejandre, R. López-Rendón, A. L. Jochim, G. J. Martyna, *J Phys A Math Gen* **2006**, *39*, 5629.

[39] W. Shinoda, M. Shiga, M. Mikami, *Phys. Rev. B* **2004**, *69*, 134103.

[40] J.-P. Ryckaert, G. Ciccotti, H. J. C. Berendsen, *J. Comput. Phys.* **1977**, *23*, 327.

[41] A. P. Thompson, H. M. Aktulga, R. Berger, D. S. Bolintineanu, W. M. Brown, P. S. Crozier, P. J. in 't Veld, A. Kohlmeyer, S. G. Moore, T. D. Nguyen, R. Shan, M. J. Stevens, J. Tranchida, C. Trott, S. J. Plimpton, *Comput. Phys. Commun.* **2022**, *271*, 108171.

[42] S. Plimpton, *J. Comput. Phys.* **1995**, *117*, 1.

[43] B. Bigot, V.-H. Peuch, *J. Phys. Chem.* **1995**, *99*, 8206.

[44] S. Furukawa, T. Nishiumi, N. Aoyama, T. Nitta, M. Nakano, *J. Chem. Eng. Jpn.* **2005**, *38*, 999.

[45] H. Sun, *J. Phys. Chem. B* **1998**, *102*, 7338.

[46] M. S. Shah, M. Tsapatsis, J. I. Siepmann, *Langmuir* **2015**, *31*, 12268.

[47] M. S. Shah, M. Tsapatsis, J. I. Siepmann, *J. Phys. Chem. B* **2015**, *119*, 7041.

[48] R. Hockney, J. Eastwood, *Computer Simulation Using Particles*, CRC Press, Boca Raton, Florida **1988**.

[49] Y. Tian, C. Yan, Z. Jin, *Sci. Rep.* **2017**, *7*, 12040.

[50] Y. Pang, X. Hu, S. Wang, S. Chen, M. Y. Soliman, H. Deng, *Chem. Eng. J.* **2020**, *396*, 125212.

[51] L. Luo, L. Zuo, Y. Wei, *Adsorpt. Sci. Technol.* **2015**, *33*, 939.

[52] O. Talu, A. L. Myers, *AIChE J.* **2001**, *47*, 1160.

[53] P. L. Llewellyn, Y. Grillet, F. Schüth, H. Reichert, K. K. Unger, *Microporous Materials* **1994**, *3*, 345.

[54] P. I. Ravikovitch, S. C. O. Domhnaill, A. V. Neimark, F. Schueth, K. K. Unger, *Langmuir* **1995**, *11*, 4765.

[55] T. Horikawa, D. D. Do, D. Nicholson, *Adv. Colloid. Interface Sci.* **2011**, *169*, 40.

[56] L. S. de Carvalho, E. Silva, J. C. Andrade, J. A. Silva, M. Urbina, P. F. Nascimento, F. Carvalho, J. A. Ruiz, *Adsorption* **2015**, *21*, 597.

[57] R. Sanz, G. Calleja, A. Arencibia, E. S. Sanz-Pérez, *Microporous Mesoporous Mater.* **2015**, *209*, 165.

[58] S. Builes, L. F. Vega, *J. Phys. Chem. C* **2012**, *116*, 3017.

[59] M. R. Oliveira, J. A. Cecilia, J. F. De Conto, S. M. Egues, E. Rodríguez-Castellón, *J. Sol-Gel Sci. Technol.* **2023**, *105*, 370.

[60] D. E. F. Oliveira, J. A. O. Chagas, A. L. de Lima, C. J. A. Mota, *Ind. Eng. Chem. Res.* **2022**, *61*, 10522.

[61] Y. Belmabkhout, A. Sayari, *Chem. Eng. Sci.* **2009**, *64*, 3729.

[62] C. A. Koh, T. Montanari, R. I. Nooney, S. F. Tahir, R. E. Westacott, *Langmuir* **1999**, *15*, 6043.

[63] P. Atkins, J. De Paula, *Atkins' Physical Chemistry*, Oxford University Press, Oxford, UK **2006**.